Supporting Information

Magnetic-actuated hydrogel microrobots with multimodal motion and collective behavior

Xi Chen[1], Chenyao Tian[1], Hao Zhang*, and Hui Xie*

The state Key Laboratory of Robotics and Systems, Harbin Institute of Technology, Harbin 150080, China

*Corresponding authors: haoz@hit.edu.cn and xiehui@hit.edu.cn.
[1]Co-first authors: Xi Chen and Chenyao Tian.

Supplementary Note I. Mechanical properties of the Ca-alginate hydrogel.

As illustrated in Fig. S1a, the tensile and compression samples of the Ca-alginate hydrogel are fabricated with the concentration of the alginate solution and the calcium solution are 0.01 and 0.05 wt. The tensile sample has a width of 5 mm, a length of 20 mm, and a thickness of 2 mm. The compression sample has a cylinder shape with a diameter of 25 mm and a height of 15 mm. The tensile and compression rates for the test are 2 mm/min. The tensile and compression results are displayed in Fig. S1b and Fig. S1c. The tensile strength and elastic modulus of the Ca-alginate hydrogel are 75.6 kPa and 49.9 kPa. The compression modulus is 17.9 kPa.

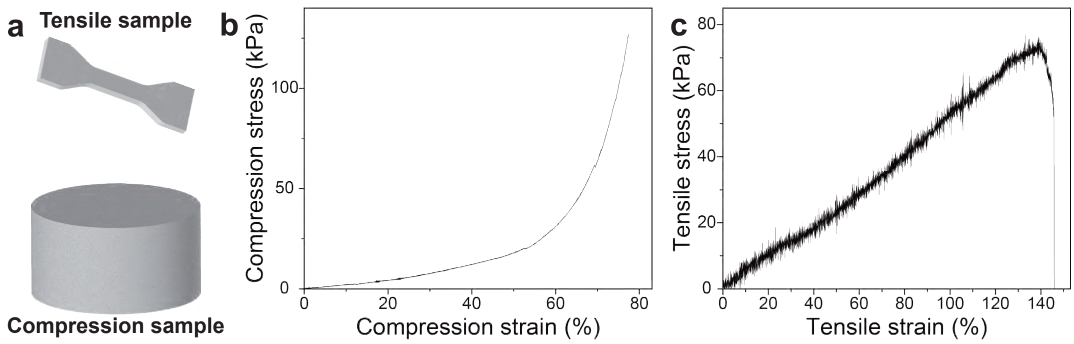

Fig. S 1. Mechanical properties of the Ca-alginate hydrogel. (a) Illustrations of samples for the mechanical tests. (b) Variation in compression stress with compression strain. (c) Variation in tensile stress with tensile strain.

Supplementary Note II. The three-dimensional network inside the MHR.

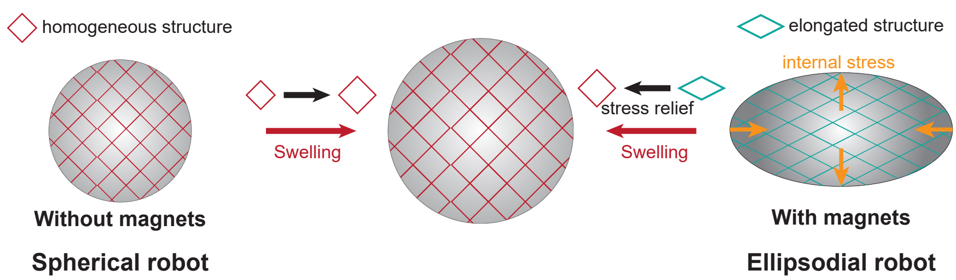

Fig. S 2. (a) Swelling behavior of the spherical robot with homogeneous structure. (b) Swelling behavior of the MHR with elongated structure.

As illustrated in Fig. S2a, the spherical hydrogel robot can be considered to possess a structure of the homogenous three-dimensional network. The swollen behavior of the spherical hydrogel can be easily predicted to form a larger sphere since its homogenous structure swells uniformly. In our proposed method, the spherical alginate droplet is first elongated to an ellipsoidal shape by the influence of magnets and then enters the calcium chloride solution to form the MHR after cross-linking. The MHR was swollen from the ellipsoidal shape to the spherical shape, indicating an elongated three-dimensional network inside the robot (Fig. S2b). With the swelling process of the MHR, the stress relief from the three-dimensional network triggered the shape deformation of the MHR.

Supplementary Note III. Simulation of the magnetic fields between the magnets.

As illustrated in Figure S3a, the permanent magnets are parallel set with a distance D. While the distance between the magnets is adjusted, the field intensities along with the y-axis are simulated and analyzed, as shown in Figure S3B. The results show that the lowest magnetic intensity appears at the center of the pair of magnets, in which the lowest intensity decreases as the distance increases. When approaching the surface of magnets, the gradient of the magnetic field becomes larger. Despite the larger distance can reduce the non-uniform property of the magnetic field, the gradient field always exists around the center area.

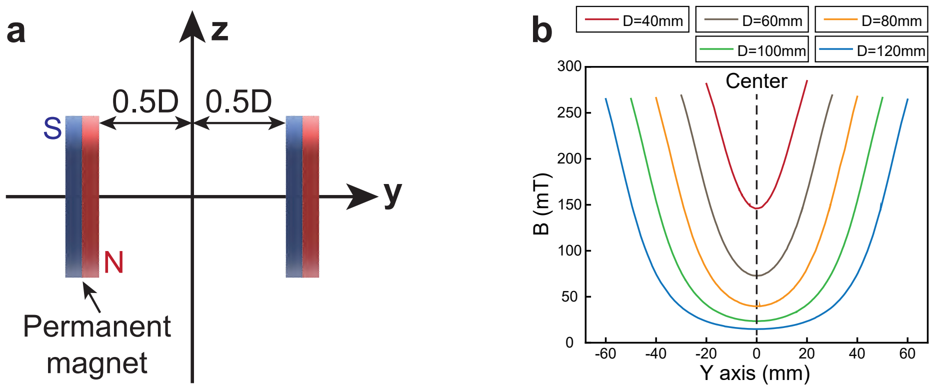

Fig. S 3. (a) Simulation setup. (b) Simulation results of magnetic field between the magnets with different distances.

Supplementary Note IV. Results of the shape deformation of the MHRs fabricated with different parameters.

A shape parameter (P) is introduced to evaluate the ellipticity of the MHRs where P represents the ratio between the length of the long-axis (a) and the length of the short-axis (b) of robots. As illustrated in Fig. S4a, several types with different P are displayed to provide a better understanding of the definition of the shape parameter. We have conducted experiments to fabricate MHRs under different concentrations of alginate solutions and magnetic fields with adjusted intensities. As shown in Fig. S4b, the MHRs fabricated by the increased concentration of alginate solution possessed less ellipticity of shapes, resulting from that the increased concentration of alginate solution had higher viscosity and limited the formation of magnetic chains. Besides, the MHRs fabricated by decreasing the distances of the magnets showed more ellipticity of shapes that derived from the larger magnetic forces between magnetic particles.

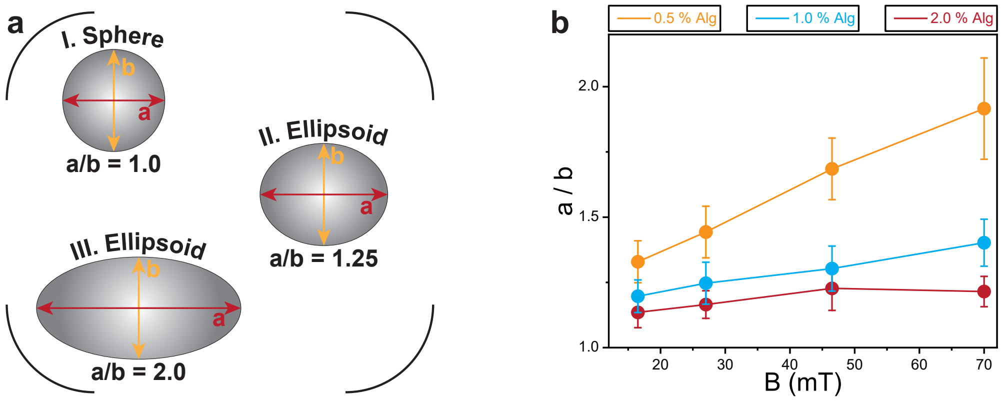

Fig. S 4. (a) Illustration of the robots with different ratios of the long-axis and the short-axis. (b) Shape parameter (P) of the robots fabricated under different concentrations of alginate solution and field intensities.

Supplementary Note V. Modification of the magnetic particles.

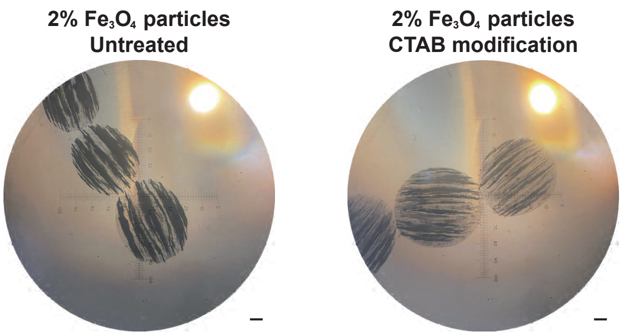

Fig. S 5. Microscopy images of the robots fabricated with untreated magnetic particles and CTAB-modified particles. Scale bars, 250 μm.

Exploiting surfactants to modify the magnetic particles is an effective method to reduce the aggregation of particles. CTAB was blended into deionized water to get a concentration of 0.1 mol/L. A certain amount of Fe_3O_4 particles was then mixed evenly with the CTAB solution with the mass ratio of Fe_3O_4 and CTAB to be 3:1. The mixture was placed in 80 °C water bath with mechanically stirring for 6 h. Finally, the magnetic particles were separated by a magnet, washed using deionized water and ethanol, and vacuum-dried at 60 °C. The surface-modified particles were exploited for the fabrication of robots. We have modified the fabrication parameters by reducing the content of magnetic particles and the speed of dripping alginate droplets for better observation of the aggregation of magnetic particles. As shown in Fig. S5, the surface-modified particles assembled into thinner chains compared to untreated magnetic particles.

Supplementary Note VI. Magnetic properties of the MHR.

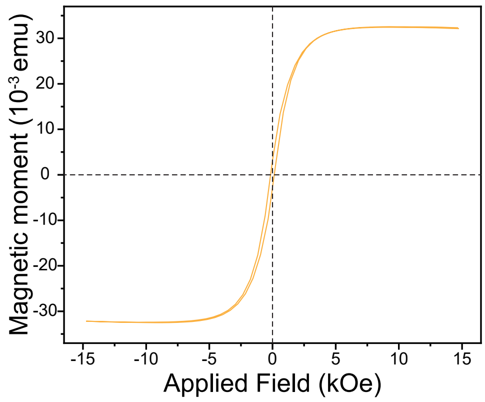

Fig. S 6. VSM data of the proposed robot.

As shown in Fig. S6, the saturation magnetization, remanence, and coercivity of the MHR are 0.032 emu, 0.0031 emu, and 140.19 Oe, respectively.

Supplementary Note VII. Velocity contrast between the spherical robot and the ellipsoidal MHR.

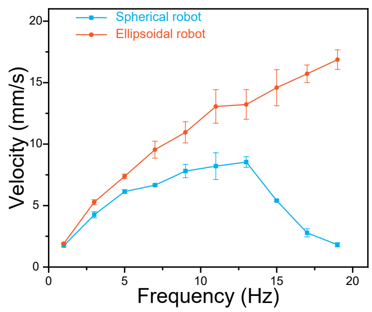

Fig. S 7. Velocity contrast between the spherical robot and the ellipsoidal MHR.

The spherical robots with a diameter of 0.62 mm and the MHR with a long-axis length of 0.84 mm and a short axis of 0.53 mm were actuated to measure their translation speeds under the rotating magnetic field of 5 mT. As shown in Fig. S7, the spherical robots reached maximum velocity at 13 Hz while the critical frequency of the MHR exceeded 19 Hz. The larger velocities of MHR in comparison with spherical robots at low frequencies were derived from the elongated axis in the robots' structure by the magnets. When the rotating magnetic field reached 19 Hz, the velocity contrast between the MHR and spherical robots was obvious and the velocities of the MHR and spherical robots were 16.86 mm/s and 1.81 mm/s, respectively. The results indicate the enhanced effect of our proposed methods on robots' motion performance.

Supplementary Note VIII. Stability tests of the dimer and trimer of the MHRs.

As shown in Fig. S8, the dimer of the MHRs (length of long-axis: 0.52 mm, length of short-axis: 0.36 mm) can be stably triggered by the magnetic field with low intensities. The trimer of the MHRs (length of long-axis: 0.52 mm, length of short-axis: 0.36 mm) is more sensitive to the intensities and frequencies of the applied magnetic fields.

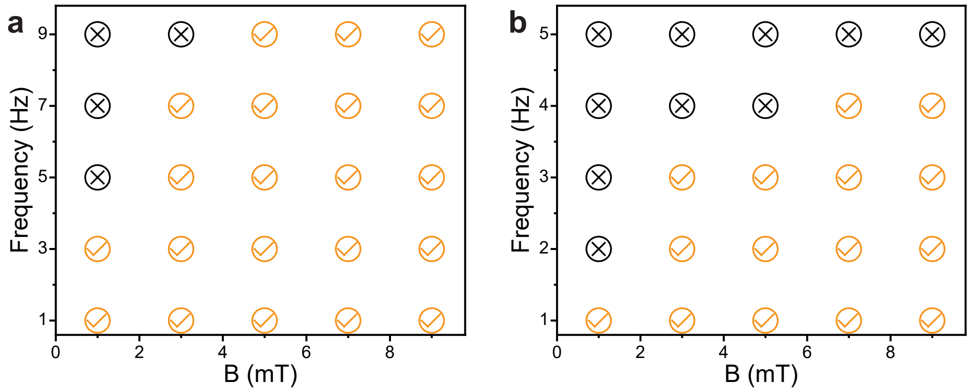

Fig. S 8. (a) Stability test of the tumbling dimer of the MHRs under different magnetic fields. (b) Stability test of the tumbling trimer of the MHRs under different magnetic fields.